Disrupted stimulus encoding shapes tactile perception in autism.

Ourania Semelidou[1,2,#], Théo Gauvrit[1,2], Célien Vandromme[1,2,3], Alexandre Cornier[1,2], Anna Saint-Jean[1,2], Yves Le Feuvre[1,2], Melanie Ginger[1,2], Andreas Frick[1,2,#]

[1] INSERM, U1215 Neurocentre Magendie, 33077, Bordeaux, France
[2] University of Bordeaux, 33000, Bordeaux, France
[3] University of Lille, 59000 , Lille, France
[#] Co-corresponding authors: ourania.semelidou@inserm.fr, andreas.frick@inserm.fr

Summary

Atypical sensory experience is an almost universal feature of autism. Amongst sensory modalities, tactile perception is particularly impacted, with alterations including difficulties detecting and discriminating low-level stimuli. However, we have not yet defined the neural underpinnings of low-level tactile perception and how they change in autism. Here we recapitulate the multifaceted tactile features of autistic individuals in the *Fmr1*$^{-/y}$ mouse model of autism and show tactile hyposensitivity and unreliable responses in a subgroup of *Fmr1*$^{-/y}$ mice. We reveal that weak stimulus encoding in the primary somatosensory cortex of *Fmr1*$^{-/y}$-hyposensitive mice renders perception vulnerable to the ongoing network state and thus unreliable. Increasing the number and reliability of stimulus-recruited neurons by targeting the large conductance calcium-activated potassium (BK_{Ca}) channels improves tactile perception. Our work shows an evolutionarily conserved role for the primary somatosensory cortex in low-level tactile perception and encompasses a highly translational approach for probing perceptual changes in neurodevelopmental conditions.

Introduction

Tactile perception is crucial to explore the world and interact with it, with the skin being the largest sensory organ. 66% of autistic individuals present alterations in tactile perception, which together with other sensory features constitute one of the core diagnostic criteria of the condition[1,2]. Apart from affecting daily life, these features also contribute to the development of other core symptoms, including difficulties in social communication and interaction and repetitive behaviors[3–5]. Tactile alterations in autistic individuals include differences in the detection and discrimination of tactile stimuli (perceptual sensitivity), overall behavioral responsivity, and sensory-related neuronal responses[6].

Studies in autistic individuals revealed the heterogeneous nature of the tactile features, reflected in the DSM-5 as "hyper- or hyporeactivity to sensory input"[7–11]. These findings extend to perception, with objective measurements of perceptual sensitivity through psychophysical approaches showing that tactile perception can be enhanced, decreased, or not affected in autistic individuals, depending on the stimulated body part and the stimulus intensity. More specifically, a study investigating the social/affiliative submodality of somatosensation with low-level forearm vibrotactile stimulation showed hypersensitivity in autistic individuals[12]. In contrast, low-level vibrotactile stimuli delivered to the fingers have revealed hyposensitivity in autistic

individuals[13,14]. However, a study using higher frequency vibrotactile stimuli to the fingers did not find any alterations in tactile detection[15].

Altered neuronal responses in the somatosensory cortex during tactile stimulation include diminished[16] or increased[17] early responses, diminished late responses[17], decreased GABA levels[18,19], and different cortical representations of tactile stimuli[20]. However, measurements of perceptual and neuronal alterations have been rarely combined, creating a knowledge gap regarding the neural correlates of altered tactile perception in autism. Moreover, technical limitations in human studies prevent the single-cell resolution measurements required to uncover the neocortical underpinnings of altered tactile perception.

Integrating psychophysics with physiological measurements provides an objective, quantifiable method for examining how sensory-related neuronal responses impact perceptual sensitivity. A psychophysical and physiological approach in the Shank3B$^{-/-}$ mouse model of autism revealed perceptual hypersensitivity to whisker stimuli[21], similar to forearm stimulation in autistic individuals[12], linked to dysfunction of GABAergic interneurons in the whisker-related primary somatosensory cortex. The similarity between the somatosensory systems of the forepaw of mice and the human hand[22–24] allows the development of a more translational model to study nuanced sensory symptomatology of autism in parallel to neuronal activity during perception.

Here we establish a standardized approach for rodent models to assess perceptual sensitivity in autism in a highly translational manner (Fig. 1a), uncover its neural correlates, and test new mechanism-based treatments. We show that the multifaceted and heterogeneous tactile features of autism can be recapitulated in the *Fmr1*$^{-/y}$ mouse model of autism, with tactile hyposensitivity, inter-individual variability, unreliable responses, and behavioral hypo-responsivity. We reveal a crucial role for the primary somatosensory cortex in the detection of low-level tactile stimuli and show weak sensory encoding in *Fmr1*$^{-/y}$-hyposensitive mice that renders tactile detection vulnerable to the ongoing network state and thus unreliable. Strengthening sensory encoding and reducing its variability through activation of the large conductance calcium-activated potassium (BK_{Ca}) channels improves tactile perception of *Fmr1*$^{-/y}$ mice.

Forepaw-based perceptual decision-making task assesses tactile detection in mice

To study the perception of vibrotactile stimuli, we back-translated a task used in human studies[13,14] and developed a Go/No-Go detection task in head-fixed mice. We combined this task with two-photon calcium imaging to examine the neural correlates of tactile perception within the primary somatosensory neocortex (S1). Water-restricted *Fmr1*$^{-/y}$ mice and their wild type (WT) littermates were trained to associate the delivery of a fixed, suprathreshold vibrotactile stimulus (15 µm, 40 Hz) with a water reward (Go trial; Fig. 1a-left). During Go trials, vibrotactile stimuli (500 ms) were delivered to the right forepaw of the mice, followed by a 2 s response window during which the mice could lick to trigger water reward delivery (Fig. 1a-left). No-Go (catch) trials in which no stimulus was presented were used to assess spontaneous licking (Fig. 1a-right).

To evaluate sensory perception, we quantified four behavioral outcomes: Hit for successful and Miss for unsuccessful Go trials, Correct Rejection (CR) for successful and False Alarm (FA) for unsuccessful No-Go trials (Fig. 1a-right). Mice completed the training period when their performance exceeded an average 70% Hit rate with less than a 30% False Alarm rate for three consecutive training days (Fig. S1a). Pre-stimulus licking (3-8 s before stimulus onset) canceled stimulus delivery and led to a 5 s timeout. 86% of the WT mice and 73% of the *Fmr1*$^{-/y}$ mice reached the aforementioned learning criterion, with no difference between the learning performances of the two groups (Fig. S1b). Similarly, no genotype effect was observed for the training duration of mice that learned the task (Fig. S1c). These data show that *Fmr1*$^{-/y}$ mice can learn the perceptual decision-making task, with a success rate and training duration similar to their WT littermates.

Fmr1$^{-/y}$ mice show perceptual hyposensitivity for low-level vibrotactile stimuli

Autistic individuals exhibit hyposensitivity to low-level (<25 µm amplitude, 25 Hz frequency) vibrotactile stimulation delivered to the fingers[13,14]. We tested whether we could replicate this phenotype in a preclinical model of autism using our translational task. We assessed the tactile sensitivity of mice that met the learning criterion during the training period by delivering novel vibrotactile stimuli of fixed frequency (10 Hz) at 6 differing amplitudes (range: 2-12 µm, 2 µm interval) in a pseudorandom manner. Mice reported the detection of a given stimulus by licking to receive a water reward. By analyzing the Hit rates for all stimulus amplitudes of sessions with low spontaneous licking (<40%), we generated psychometric curves (Fig. 1b) enabling us to determine the detection threshold (stimulus amplitude detected in 50% of the trials), perceptual accuracy (curve slope), and licking strategy (criterion c') for each mouse.

Fmr1$^{-/y}$ mice exhibited decreased tactile sensitivity (Hit rates) across the entire amplitude range (Fig. 1b), resulting in increased detection thresholds (Fig. 1c) and a trend for lower perceptual accuracy (Fig. S1d) compared to their WT littermates. This difference in detection was not due to alternative strategies adopted by the mice to obtain the reward, as indicated by the similar values of the criterion c' (Fig. S1e). Our results recapitulate the findings in autistic individuals, with *Fmr1*$^{-/y}$ mice showing perceptual hyposensitivity to low-level vibrotactile stimulation.

Fmr1$^{-/y}$ mice show increased interindividual variability during tactile detection

High interindividual variability in behavior and sensory stimulus-evoked neural responses has emerged as a hallmark of autism over the last 15 years[17,25–28]. We examined differences in interindividual variability in our mouse model by comparing the group variance of the Hit rates for each amplitude. Our results show higher interindividual variability in the *Fmr1*$^{-/y}$ group compared to WT mice, with a statistically significant increase in variance observed for all stimuli exceeding the amplitude of 4 µm (Fig. 1d).

Further inspection of the responses of *Fmr1*$^{-/y}$ mice suggested the existence of discrete subgroups. We therefore used K-means clustering on the Hit rates of *Fmr1*$^{-/y}$ mice to divide this cohort into two subgroups. Consistent with findings from autistic individuals[26], one subgroup of *Fmr1*$^{-/y}$ mice exhibited tactile stimulus detection comparable to that of WT mice, while the second subgroup displayed diminished tactile sensitivity across all stimulus amplitudes (here referred to

as *Fmr1*$^{-/y}$-hyposensitive mice; Fig. 1e). This reduced sensitivity of *Fmr1*$^{-/y}$-hyposensitive mice is evidenced by an elevated perceptual detection threshold (Fig. 1f) and decreased perceptual accuracy (cf. *Fmr1*$^{-y}$ and WT group) (Fig. 1g). Importantly, no genotype differences were observed in strategy (Fig. 1h) and learning abilities (Fig. 1i, Fig. S1f).

Intrigued by the perceptual differences within the *Fmr1*$^{-/y}$ cohort, we explored possible causes for this phenotypic heterogeneity. We first verified that mice of both subgroups belonged to the same litters and controlled for the age of parents and the order of the litter, thus excluding the possibility of litter- or breeder-specific variability[29]. We also verified that there was no difference in the size of the litter between the two groups, which positively correlates with behavioral alterations in mice[30] (Fig. S1g). Finally, we measured the body weight, which inversely correlates with sensitivity to visual stimuli in vertebrates[31], as does metabolic rate in humans[32]. *Fmr1*$^{-/y}$-hyposensitive mice weighed 2.5 g more than the WT animals before water restriction, a difference that was not observed between WT mice and the other *Fmr1*$^{-/y}$ subgroup (Fig. S1h). Noteworthy, metabolic alterations have previously been described in the context of autism[33–37].

These results demonstrate an increased interindividual variability within the *Fmr1*$^{-/y}$ cohort, with tactile hyposensitivity in one subgroup of *Fmr1*$^{-/y}$ mice that also exhibits increased body weight.

Increased intra-individual variability across stimulus trials in *Fmr1*$^{-/y}$-hyposensitive mice

Intra-individual variability has been observed in the behavioral responses of autistic individuals to tactile and visual stimuli[8,38,39], and in their neuronal responses to tactile, visual and auditory stimulation[40–42]. Our results of altered perceptual accuracy among the *Fmr1*$^{-/y}$-hyposensitive mice (Fig. 1g) suggest less reliable responses in these animals. To further investigate this idea, we assessed the trial-by-trial (TBT) variability in the behavioral response for each stimulus amplitude in Go trials. Response variability increased close to threshold stimulation for WT mice and *Fmr1*$^{-/y}$ mice with intact perception (Fig. 1j). However, *Fmr1*$^{-/y}$-hyposensitive mice exhibited increased TBT variability for all stimulus amplitudes higher than 6 µm and increased mean variance of responses compared to the other groups (Fig. 1j).

To examine genotype differences in response variability for threshold and non-threshold stimuli, we analyzed the TBT variability of responses at the threshold amplitude (50% Hit rate), as well as the first sub-threshold and supra-threshold amplitudes for each mouse. As expected, all groups showed a large TBT variability for responses to the threshold amplitude, but the *Fmr1*$^{-/y}$-hyposensitive mice exhibited significantly less reliable responses for both sub- and suprathreshold amplitudes (Fig. 1k). These data show unreliable responses in *Fmr1*$^{-/y}$-hyposensitive mice across sub- and supra-threshold stimuli, reproducing one of the hallmark characteristics observed in autistic individuals.

***Fmr1*$^{-/y}$ mice present behavioral hypo-responsivity in response to tactile stimulation**

There is a growing appreciation of the heterogeneous nature of sensory features that include not only differences in perceptual sensitivity, but in the overall behavioral responsivity as well[6]. We probed alterations in behavioral responsivity to tactile stimulation in *Fmr1*$^{-/y}$ mice by employing an adhesive removal task[43]. In this task, we attached an adhesive tape to each forepaw of the mice and measured the time they took to make their first contact with the tape. This delay

assesses the behavioral responsivity of mice to a prolonged, non-aversive, non-sinusoidal stimulation. *Fmr1*$^{-/y}$ mice showed hypo-responsivity, with a longer delay to their first contact with the adhesive tape (Fig. 1l). In contrast, no motor deficits were identified, since both groups required the same time to remove the adhesive tape after the first contact (Fig. 1l).

Weak stimulus encoding in *Fmr1*$^{-/y}$-hyposensitive mice

To explore the neural correlates of tactile perception in WT and *Fmr1*$^{-/y}$ mice, we recorded responses of populations of excitatory pyramidal neurons and inhibitory GABAergic interneurons in the forepaw-related primary somatosensory cortex (S1-FP) during tactile detection (Fig. 2a). The total number of recorded pyramidal neurons and inhibitory interneurons in the field of view did not differ across genotypes (Fig. S2a-b). Neuronal activity was then aligned with tactile stimulation and behavioral response, enabling us to explore the neural dynamics underlying stimuli of different amplitudes, detected or non-detected (Fig. 2b).

According to psychophysics and signal detection theory, stimulus perception results from two functions, one describing the stimulus transformation and another the response transformation[44,45]. In our task, the stimulus transformation function translates the physical characteristics of the stimulus (amplitude) into a perceptual magnitude (stimulus encoding). The response transformation function calculates the difference between the perceptual magnitude and noise levels to generate a behavioral response (response decoding). To assess how each stimulus amplitude is encoded in S1-FP, we calculated the percentage of activated and inhibited neurons during stimulation. We found an increased number of activated pyramidal neurons and GABAergic interneurons as the stimulus amplitude increased, across all groups (Fig. 2c). While the percentage of inhibited pyramidal neurons did not increase with higher stimulus amplitudes, more GABAergic interneurons were inhibited as the stimulus amplitude increased (Fig. 2d).

Given that stimuli with higher amplitude are more easily detected, the ratio of detected to non-detected trials varies across the range of amplitudes. To assess if neural responses encode for amplitude, we compared the number of recruited (activated or inhibited) pyramidal neurons and GABAergic interneurons during detected trials for each amplitude. Our results show an effect for stimulus amplitude in activated pyramidal neurons (Fig. 2e-top) but not in activated GABAergic interneurons (Fig. 2e-bottom), inhibited pyramidal neurons (Fig. S2c-top), or inhibited GABAergic interneurons (Fig. S2c-bottom).

Between-group comparisons showed that *Fmr1*$^{-/y}$-hyposensitive mice presented significantly less activation of pyramidal neurons and GABAergic interneurons for most stimulus amplitudes, reaching WT levels only for the highest amplitude of 12 µm (Fig. 2c). Levels of inhibited neurons were similar between all groups (Fig. 2d). Interestingly, we saw no genotype effect in the number of activated neurons during detected trials (Fig. 2e), similar to our previous observation for the 12 µm amplitude that is detected with higher probability (Fig. 2c). *Fmr1*$^{-/y}$ mice with typical tactile detection did not present any alterations in the number of recruited neurons compared to their WT littermates (Fig. 2c-e).

To test whether the neuronal responses were stimulus-specific, we compared the percentage of recruited neurons during the No-Go (catch) trials between *Fmr1*$^{-/y}$-hyposensitive and their WT

littermates. Our data showed similar recruitment of pyramidal neurons and GABAergic interneurons between the two groups (Fig. S2d), independently of the behavioral outcome (FA or CR) (Fig. S2e-f).

Taken together, these results show that encoding of stimulus amplitude in S1-FP is related to the number of activated pyramidal neurons across all groups. *Fmr1*$^{-/y}$-hyposensitive mice show significantly decreased neuronal activation, resulting in weaker perceptual magnitude that correlates with their perceptual hyposensitivity (Fig. 1f-g). In contrast, no differences were observed in the neuronal responses of the *Fmr1*$^{-/y}$ mice with typical tactile detection, supporting their intact perceptual performance.

Fmr1$^{-/y}$-hyposensitive mice show altered neuronal responses during tactile detection

To investigate whether stimulus encoding differs between detected and non-detected trials, we compared the number of recruited pyramidal neurons and GABAergic interneurons for each behavioral response regardless of stimulation intensity, in WT and *Fmr1*$^{-/y}$-hyposensitive mice. We found five times more activated pyramidal neurons during detected trials (cf. non-detected trials) in WT mice and three times more in *Fmr1*$^{-/y}$-hyposensitive mice (Fig. 2f-top). In WT mice this increased activation during detection was accompanied by an augmentation of the percentage of inhibited pyramidal neurons and GABAergic interneurons (Fig. 2g). Surprisingly, even though *Fmr1*$^{-/y}$-hyposensitive mice displayed increased activation of GABAergic interneurons during detection (Fig. 2f-bottom), they did not show strong detection-related inhibition (Fig. 2g). Comparison of recruited neurons between the two groups showed a strong trend of less stimulus-recruited pyramidal neurons during detected stimuli in *Fmr1*$^{-/y}$-hyposensitive mice (Fig. S2g). These results show a stronger perceptual magnitude for detected stimuli compared to non-detected ones, in both groups. However, the perceptual magnitude during detection was weaker in the *Fmr1*$^{-/y}$-hyposensitive mice, which did not exhibit stimulus-related inhibition, even though they showed more activated GABAergic interneurons during detection.

Stronger and faster responses during tactile detection in WT but not in _Fmr1_$^{-/y}$-hyposensitive mice

In addition to the number of recruited neurons, the perceptual magnitude can also be determined by the amplitude or the time course of the neuronal responses. To investigate possible differences in the amplitude of neuronal responses between detected and non-detected trials, we calculated the peak amplitude of recruited neurons during stimulation. We found a slight but significant increase in the response amplitude of activated pyramidal neurons and a trend in inhibited GABAergic interneurons during detection in WT mice, which was not mirrored in the *Fmr1*$^{-/y}$-hyposensitive group (Fig. 2h-i).

To examine whether neuronal responses had a different response delay for detected trials we measured the latency of the peak amplitude from the stimulus onset. Our results show faster responses in recruited pyramidal neurons during detected trials in WT mice, but not in *Fmr1*$^{-/y}$-hyposensitive mice (Fig. 2j-k). These data demonstrate a higher response amplitude and faster responses during detected trials in WT but not *Fmr1*$^{-/y}$-hyposensitive mice.

Perceptual magnitude determines response decoding of threshold stimuli in WT but not in *Fmr1*$^{-/y}$-hyposensitive mice

Our results show that detected stimuli of all amplitudes recruit more neurons in S1-FP compared to non-detected stimuli. To better understand how perceptual magnitude impacts response generation we focused on threshold stimuli, where the same stimulus amplitude is detected in ~50% of the trials. We found that for threshold stimuli, WT mice showed five times more activated neurons when the stimulus was detected compared to when it was not, while this was not observed in Fmr1$^{-/y}$-hyposensitive mice (Fig. 3a). Conversely, the response amplitude and delay were not different between detected and non-detected threshold trials (Fig. S3a-b), indicating that perceptual magnitude for threshold stimuli is primarily encoded by the number of activated neurons in WT mice and not their amplitude or time course.

Fmr1$^{-/y}$-hyposensitive mice showed a trend for more activated neurons during detected threshold stimuli compared to non-detected ones (Fig. 3a). However, the recruitment of pyramidal neurons during detection was significantly lower compared to WT mice (Fig. 3c). Similarly, the difference in the recruited pyramidal neurons between detected threshold trials and No-Go trials was decreased in *Fmr1*$^{-/y}$-hyposensitive mice compared to their WT littermates (Fig. S3c-Detected).

Taken together, our results show that the number of activated pyramidal neurons generates the perceptual magnitude during threshold stimulation, which in turn determines response decoding in WT mice. In contrast, the weak perceptual magnitude in *Fmr1*$^{-/y}$-hyposensitive mice has less impact on response decoding.

Response decoding in *Fmr1*$^{-/y}$-hyposensitive mice is contingent upon the ongoing network state

In the framework of response transformation, weak perceptual magnitude (Fig. 2c-d, Fig. 3a-c) suggests a strong impact for noise in response decoding. Increased endogenous neural noise correlates with enhanced trial-by-trial (TBT) variability of the neuronal responses of the primary somatosensory cortex in *Fmr1*$^{-/y}$ mice[46]. Moreover, our behavioral results showed high TBT variability in *Fmr1*$^{-/y}$-hyposensitive mice (Fig. 1j-k). We thus computed the average z-score response of each threshold trial during stimulation, and examined TBT variability by calculating a measure of similarity (cosine similarity) between each pair of threshold trials for each mouse. Our results showed higher TBT variability in the responses of pyramidal neurons during detected threshold stimuli in *Fmr1*$^{-/y}$-hyposensitive mice (Fig. 3d).

Increased TBT variability can be the result of different neurons recruited across trials. To investigate this, we identified the recruited pyramidal neurons at threshold stimulus from trial to trial. Our results demonstrate that recruitment of specific pyramidal neurons across trials shows similar TBT variability in WT and *Fmr1*$^{-/y}$-hyposensitive mice, with ~40% of detected trials recruiting the same neurons (Fig. 3e).

We then examined if the increased TBT variability preferentially resulted from the responses of so-called driver neurons — neurons that reliably respond to the stimulus and are recruited in >5 detected stimulus trials. Our analysis revealed that *Fmr1*$^{-/y}$-hyposensitive mice exhibit elevated TBT variability in the responses of both driver and non-driver neurons (Fig. 3f-g) and have fewer driver neurons compared to their WT littermates (Fig. 3h).

Finally, we investigated the impact of the pre-stimulus activity of pyramidal neurons on stimulus-related responses[46,47] by probing the correlation of TBT variability in pre-stimulus activity (average activity during 500 ms before stimulus onset) with that during threshold stimulation. Our results demonstrate that the pre-stimulus TBT variability positively correlates with stimulus TBT variability in WT but not in *Fmr1*$^{-/y}$-hyposensitive mice (Fig. 3i). Thus, stimulus encoding is variable in *Fmr1*$^{-/y}$-hyposensitive mice independently of the baseline variability before stimulation.

Collectively, these data demonstrate that response decoding in *Fmr1*$^{-/y}$-hyposensitive mice is highly contingent upon the network state during stimulation and shows increased TBT variability. In contrast, strong and reliable stimulus encoding into a perceptual magnitude in WT mice makes response decoding less vulnerable to the influence of noise within the network.

Fmr1$^{-/y}$-hyposensitive mice show increased excitation-to-inhibition ratio in non-detected trials

Reduced inhibition in the neocortex shifts the balance towards excitation, leading to noisier or more unreliable information processing in autism[48]. We previously observed increased detection-related inhibition in WT but not in *Fmr1*$^{-/y}$-hyposensitive mice (Fig. 2g). We thus examined whether *Fmr1*$^{-/y}$-hyposensitive mice showed differences in their excitation-inhibition (E/I) ratio. While we did not observe general E/I ratio alterations in *Fmr1*$^{-/y}$-hyposensitive mice during detected trials (Fig. 3j) and No-Go trials (Fig. S3d), non-detected trials were characterized by an increased E/I ratio in these mice (Fig. 3j). These results, combined with low activation of GABAergic interneurons in *Fmr1*$^{-/y}$-hyposensitive mice during non-detected trials (Fig. 2f), indicate decreased inhibition during non-detected stimuli in *Fmr1*$^{-/y}$-hyposensitive mice. Thus, E/I ratio alterations lead to a noisier network compared to WT mice in a context-dependent manner, that might explain reduced stimulus detection.

Unreliable stimulus encoding impedes response decoding in _Fmr1_$^{-/y}$-hyposensitive mice

To further explore the variations in response decoding between WT and *Fmr1*$^{-/y}$-hyposensitive mice, we employed dynamic decoding classifiers through a logistic regression model. We trained the model on each acquisition frame (32 ms) of pre-stimulus (1 s) and stimulus-related (500 ms) neuronal activity datasets of each mouse[47], to predict stimulus detection based on neuronal activity (Fig. 4a). Our model successfully differentiated detected from non-detected trials in WT mice (Fig. 4b) but performed worse when trained with datasets of *Fmr1*$^{-/y}$-hyposensitive mice (Fig. 4c). Comparisons of the decoding accuracy during stimulus delivery between the two groups showed a strong trend for less accurate predictions of detected trials in *Fmr1*$^{-/y}$-hyposensitive mice (Fig. 4d). This effect was exacerbated when comparing the accuracy of the model during the last 250 ms of the stimulus (Fig. 4e), an approach that considers evidence accumulation during stimulus delivery[49].

Pre-stimulus TBT variability positively correlated with stimulus-related TBT variability in WT mice (Fig. 3i). We thus calculated the decoding accuracy of our model during the last 200 ms of the pre-stimulus period, close to stimulus onset. We observed a performance above chance level in predicting detected stimuli in WT mice, but not in *Fmr1*$^{-/y}$-hyposensitive mice (Fig. 4f), confirming that pre-stimulus activity influences stimulus detection in WT mice.

To investigate the origin of the decreased decoding accuracy in *Fmr1*$^{-/y}$-hyposensitive mice, we examined the impact of TBT variability on decoding accuracy. We found a positive correlation between TBT similarity and model accuracy in WT mice and a strong trend in *Fmr1*$^{-/y}$-hyposensitive mice (Fig. 4g). In contrast, there was no correlation between the model accuracy and the number of recruited neurons (Fig. 4h) or consistently responding driver neurons (Fig. 4i), indicating that the activity of few, reliable neurons is sufficient for the model to predict behavioral responses. These results show that increased TBT variability impacts response decoding, rendering it less accurate in *Fmr1*$^{-/y}$-hyposensitive mice.

Altogether, our results show reliable response decoding based on perceptual magnitude and influenced by pre-stimulus activity in WT mice. In contrast, increased TBT variability in *Fmr1*$^{-/y}$-hyposensitive mice impedes response decoding.

Tactile sensitivity is improved upon treatment with a BK_{CA} agonist in *Fmr1*$^{-/y}$ mice

Large conductance voltage- and calcium-sensitive potassium (BK_{Ca}) channel dysfunction has been associated with neurodevelopmental disorders such as autism spectrum disorder and fragile X syndrome[50–52]. Application of BK_{Ca} channel agonists can reverse neuronal and behavioral alterations in *Fmr1*$^{-/y}$ mice[46,53–55]. We examined whether BK_{Ca} channel dysfunction also contributes to tactile hyposensitivity of *Fmr1*$^{-/y}$ mice (both typically detecting and hyposensitive, Fig. 1b-c) and can be corrected upon treatment. The BK_{Ca} channel agonist, BMS-204352 (BMS), or its vehicle (DMSO) was delivered by intraperitoneal injection 30-45 minutes before tactile detection testing. Our results demonstrate that activating BK_{Ca} channels improved tactile sensitivity in *Fmr1*$^{-/y}$ mice (Fig. 5a-c), which showed similar detection thresholds to their WT littermates (Fig. 5d). Treatment also eliminated the difference in the perceptual accuracy between the groups (Fig. 5e), but did not affect the licking strategy (Fig. 5f). Our results demonstrate that activation of BK_{Ca} channels improves perceptual thresholds in *Fmr1*$^{-/y}$ mice.

Treatment with a BK_{CA} agonist enhances stimulus encoding in *Fmr1*$^{-/y}$ mice

To examine whether restored BK_{Ca} channel function also improves stimulus encoding in *Fmr1*$^{-/y}$ mice, we analyzed neuronal responses during tactile detection upon BMS treatment. We observed that BMS treatment enhanced stimulus encoding in *Fmr1*$^{-/y}$ mice (Fig. 5g). Under BMS treatment, we found only a trend for reduced percentage of activated pyramidal neurons during detected trials between WT and Fmr1$^{-/y}$ mice (Fig. 5h-top), but no change in the percentage of activated GABAergic interneurons (Fig. 5h-bottom) or the percentage of inhibited neurons (Fig. S4a). Remarkably, under BMS the differentiation between detected and non-detected trials was similar in *Fmr1*$^{-/y}$ and WT mice. This was evidenced as the percentage of activated pyramidal neurons and GABAergic interneurons (Fig. 5i) and the percentage of inhibited GABAergic interneurons (Fig. S4b). Moreover, upon BMS treatment the number of activated driver pyramidal neurons in detected trials was similar between *Fmr1*$^{-/y}$ and WT mice (Fig. 5j). However, no difference was observed in the number of recruited neurons during non-detected trials between WT and *Fmr1*$^{-/y}$ mice (Fig. S4c). We next examined if BMS treatment also modulated TBT variability. Surprisingly, we found a trend for increased TBT variability upon BMS treatment in *Fmr1*$^{-/y}$ mice (Fig. S4d), further confirmed by high TBT variability in the responses of non-driver neurons upon stimulation (Fig. S4e). Collectively, our results show that BMS treatment enhanced

stimulus encoding, allowing a stronger and more reliable perceptual magnitude to determine response decoding and render it less contingent upon the network state.

Discussion

In this study we tackle the challenge of experimentally mimicking the nuanced and heterogeneous features of autistic individuals in transgenic mouse models[56] by back-translating a psychophysical task used in human studies. Our results from a mouse model of autism demonstrate a remarkable fidelity in capturing the nuances of altered sensory perception in autism, such as tactile hyposensitivity[13,14], high interindividual variability[17,25,27,28], unreliable responses[8,38,39] and hypo-responsiveness[7,10]. Consistent with human studies[57,58], these tactile symptoms were not linked with cognitive deficits.

Tactile perception alterations in autism depend both on the tactile sub-modality and the body part that receives the stimulus, revealing hypo- or hypersensitivity in autistic individuals[12–14]. Our findings of tactile hyposensitivity in *Fmr1*$^{-/y}$ mice are consistent with studies of the same mouse model using forepaw-dependent discrimination tasks[59,60] and show the importance of the tactile sub-modality in behavioral responsivity[61]. Conversely, whisker stimulation revealed hypersensitivity in the *Shank3B*$^{-/-}$ mouse model[21] and hyper-responsiveness in *Fmr1*$^{-/y}$ mice[62].

Intriguingly, we reveal a subgroup of *Fmr1*$^{-/y}$ mice with tactile hyposensitivity. This result was unexpected for an inbred mouse line but supports the existence of sensory subgroups with different tactile features in autism[58] and underlines the relevance of addressing inter-individual variability in autism research. The increased body weight of the hyposensitive-*Fmr1*$^{-/y}$ subgroup suggests that metabolic alterations in autism[33–37,63–65] might impact the metabolic rate in S1-FP and thus tactile sensitivity[31,32].

At the neuronal network level, we show that the role of the forelimb-related primary somatosensory cortex in tactile detection in humans[66–68] is evolutionarily conserved in mice. We demonstrate that encoding of vibrotactile stimuli within the forepaw-related primary somatosensory cortex (FP-S1) in mice generates perceptual magnitudes through both activation and inhibition of pyramidal neurons. Activated and inhibited neuronal ensembles were recently described during stimulus encoding in the visual cortex of mice[69]. We observed that sparse stimulus encoding in FP-S1 is sufficient to lead to detection[70]. A previous study suggested that stimulus detection depends on the signal-to-noise ratio in S1[47]. Here we confirm this, showing that the perceptual magnitude generated through the encoding of detected stimuli was different to that of non-detected ones. During ambiguous threshold stimuli, detection depends on the number of activated pyramidal neurons. We further validate that noise/variability in S1 affects detection[47,71], evidenced by the effect of prestimulus activity in stimulus encoding and response decoding. Finally, neuronal responses in the FP-S1 during stimulation are sufficient to decode the behavioral response to the stimulus, congruent with results from the barrel cortex[72,73].

We reveal that weak and unreliable stimulus encoding in *Fmr1*$^{-/y}$-hyposensitive mice generates a weak perceptual magnitude and makes response decoding highly contingent upon the ongoing network state. Indeed, we link alterations in the E/I ratio, an indicator of the balance in the network state, with perceptual sensitivity and demonstrate an increased E/I ratio during non-

detected trials in *Fmr1*$^{-/y}$ mice. Increased E/I ratio was previously shown in autistic individuals and mouse models of autism[19,48,74], and decreased GABA levels have been correlated with tactile perception[18]. Reduced somatosensory responses were previous reported in autistic individuals[16,17] and in the *Syngap1*$^{+/-}$ mouse model of autism, where they were linked to reduced synaptic connectivity and impaired intrinsic excitability[75]. However, *Fmr1*$^{-/y}$ mice show circuit hyperexcitability in primary sensory cortices[46,53,76]. We suggest that perceptual magnitude is dampened and tactile detection is undermined in *Fmr1*$^{-/y}$ mice as a result of hyperexcitability and its effect on canonical computations, like divisive normalization[77]. Hyperexcitability in FP-S1 in *Fmr1*$^{-/y}$ mice reduces the signal-to-noise ratio during stimulation, with the stimulus-related information that arrives in each neuron being normalized over the non-stimulus related inputs that rise from the hyperexcitable network. This results in decreased number of stimulus-recruited neurons in *Fmr1*$^{-/y}$-hyposensitive mice and increased response variability that depends on the ongoing network state and has been proposed as a hallmark of autism[40–42,46,78].

Administration of a BK_{Ca} channel agonist[46,53–55,79] ameliorates tactile detection in *Fmr1*$^{-/y}$ mice by strengthening the perceptual magnitude and its reliability. We speculate that reduced spontaneous firing activity upon treatment[46] increases the signal-to-noise ratio through increased weight of the stimulus-related input at the S1-FP neurons. Even though targeting BK_{Ca} channels can restore some aspects of trial-by-trial variability in single neuron responses in *Fmr1*$^{-/y}$ mice[46], we did not observe the same effect at the network level.

We reveal tactile heterogeneity in perceptual and neuronal responses in a mouse model of autism and demonstrate that tactile hyposensitivity stems from weak and unreliable stimulus encoding in the primary somatosensory cortex. This renders response decoding more vulnerable to the noisy network state. Our work advocates for subject classification into subgroups based on sensory features, both in human studies[58,80,81], and in preclinical models of autism. This stratification is crucial for evaluating novel treatments in preclinical and clinical studies, facilitating personalized treatment[82].

Materials and Methods

Experimental design

We back-translated a task used in human studies[13] and developed a novel Go/No-go detection task for vibrotactile stimuli which we combined with two-photon calcium imaging of excitatory and inhibitory neurons in the forepaw-related primary somatosensory cortex (FP-S1) to study altered tactile perception in autism and define its neural correlates. Throughout the text, we are using terms that are preferred in the autistic community and are less stigmatizing.

Ethical statement

All experimental procedures were performed in accordance with the EU directive 2010/63/EU and French law following procedures approved by the Bordeaux Ethics Committee and Ministry for Higher Education and Research. Mice were maintained in reversed light cycle under controlled conditions (temperature 22–24 °C, humidity 40–60%, 12 h/12 h light/dark cycle, light on at 21:00)

in a conventional animal facility with ad libitum access to food and ad libitum access to water before the water restriction period. All experiments were performed during the dark cycle, under red light.

Mice

Second-generation *Fmr1* knockout (*Fmr1*$^{-/y}$) and wild-type littermate mice 5-16 weeks old were used in our study. Mice were maintained in a mixed 129/Sv/C57Bl/6 J/FVB background (backcrossed 6 generations into C57Bl/6J) as described in ref.[46,53]. Male wild-type and *Fmr1*$^{-/y}$ littermates were generated by crossing *Fmr1*$^{+/-}$ females with *Fmr1*$^{+/y}$ male mice from the same production, and the resulting progeny used for our experiments was either *Fmr1*$^{+/y}$ (wild type) or *Fmr1*$^{-/y}$ (KO). Mice were maintained in collective cages following weaning (2-4 litter males per cage). Cages were balanced for genotype and supplemented with cotton nestlets and carton tubes. Number of mice are given in the figure captions. The genotype of experimental animals was re-confirmed post hoc by tail-PCR.

Surgery

Mice (P33-42) were anaesthetized with isoflurane (4.5% induction, 1.5-2% maintenance). Proper depth of anesthesia was monitored by testing the absence of a foot-pinch reflex and whisker movement. Mice were head-fixed using non-puncture ear-bars and a nose-clamp, and optic gel (Ocry-gel) was applied to both eyes. Body temperature was maintained at 37 °C with a heating pad and rectal probe. Prior to the beginning of the surgery, saline (0.1 ml/ 10 g) and 0.1 ml of a 1:10 Buprenorphine to saline solution were administered subcutaneously. Following hair trimming and application of Betadine scrub and Betadine dermal solution at the scalp, 0.1 ml of a 1:4 Lidocaine to saline solution was administered subcutaneously and waited for 2–5 min to induce local analgesia. The scalp was carefully removed and a 3 mm diameter craniotomy was made above the S1 forepaw region (0.75 mm anterior and -2.5 mm lateral from Bregma, confirmed with intrinsic imaging coupled with forepaw stimulation) using a dental drill (World Precision Instruments). The cortical surface was rinsed with saline throughout the surgery. Stereotactic injections of 100 nl of AAV1/2-syn-jGCaMP8m (titre: 2.6E+12 gcp/ml, diluted 1:4 in Hank's Balanced Salt Solution) and AAV1/2-mDlx-HBB-chI-mRuby3-SV40p(A) (titre: 8.6E+13 gcp/ml, diluted 1:2 in Hank's Balanced Salt Solution) were delivered (50 nl/ min) in layers 2/3 (z depth 0.3mm). A double coverslip, composed of a 3 mm diameter lower glass and a 4 mm diameter upper glass glued together with optical adhesive (NOA 61, Norland Products), was implanted on top of the craniotomy and secured in place with cyanoacrylate glue. A head-post was attached to the skull with cyanoacrylate glue and secured with dental cement. An optical glue (OptiBond Universal, Kerr) and dental filling material (Charisma, Kulzer) were applied on the skull and curated with LED blue light. Dental cement was applied on the top. After the surgery the mice were placed on a warm blanket for 1 h after they awoke from anesthesia.

Go/No-Go vibrotactile decision-making task

Setup

The vibrotactile decision-making setup was positioned in an isolation cubicle to minimize interference during the experiment. Mice were placed in a body tube and were head-fixed with

their forepaws resting on two steel bars (6 mm diameter, Thorlabs). The right bar was mounted to a Preloaded Piezo Actuator (P-841.6, Physik Instrumente) equipped with a strain gauge feedback sensor and controlled (E-501, Physik Instrumente) in a closed loop, as described before[83]. Water reward was delivered through a metal feeding needle (20G, 1,9mm tip, Agntho's AB) connected to a lickport interface with a solenoid valve (Sanworks) equipped with a capacitive sensor (https://github.com/poulet-lab/Bpod_CapacitivePortInterface). The behavioral setup was controlled by Bpod (Sanworks) through scripts in Python (PyBpod, https://pybpod.readthedocs.io/en/latest/).

Habituation to head-fixation and water restriction

Mice (P40-P50) were handled using carton tubes and the cupping technique until they were comfortable in the experimenter's hands, attested by eating while handled. Mice were gradually habituated to the experimental setup and head fixation for 5 days. The third day of habituation, a water-restriction protocol was implemented, where mice had access to liquid water in the setup and to a solid water supplement (Hydrogel, BioServices) in their home cage. In total, the animals received 1.5-2 ml of water per day, which corresponds to 50-65% of their ad libitum consumption, while ensuring that they did not lose more than 10% of their weight. Each mouse received 6-8 g of Hydrogel (ad libitum) during the weekend. This water restriction protocol was maintained throughout behavioral training and until the end of behavioral testing.

Go/No-Go vibrotactile task training and testing

Habituated mice (8 weeks old) were trained to associate vibrotactile stimulus delivery (pure sinusoid, 500 ms duration, 15 µm amplitude, 40 Hz frequency) with a water reward (8 µl). Go trials consisted of stimulus delivery followed by a 2 s response window during which the mice could lick to receive the reward. No-Go (catch) trials included no stimulation and licking during these trials resulted in a 5 s timeout before the beginning of the following trial. Inter-trial intervals were variable (5-10 s). Training was subdivided in 3 phases: (a) automatic water delivery at the beginning of the response window (b) Pre-training: lick-triggered water delivery during Go trials and timeout delivery during No-Go trials (c) Training: lick-triggered water delivery during Go trials when the mouse did not lick during the inter-trial interval (3-8 s) before the stimulation. No stimulus delivery and timeout (5 s) if the animal licked during the inter-trial interval (3-8 s) before the stimulus and timeout delivery (5 s) during No-Go trials. All sessions consisted of 300 trials with 70-80% Go and 20-30% No-Go proportion. All trials were presented in a pseudorandom sequence. Pilot experiments with an extra sensor to monitor forepaw placement confirmed that the mice did not remove their forepaws from the bar before stimulus delivery. To complete Pre-training, mice needed to complete 80% of successful Go trials and reduce their spontaneous licking during No-Go trials below 40%. To complete Training, mice needed to reach the criterion of more than 80% successful Go-trials and less than 30% unsuccessful No-Go trials as an average for 3 consecutive days. All mice that fulfilled this criterion were tested for the detection of vibrotactile stimuli of differing amplitudes that they haven't experienced before. During testing a 90% Go:10% No-Go ratio was delivered. Go trials consisted of 6 vibrotactile stimuli (pure sinusoid, 500 ms duration, 10 Hz frequency, 2-4-6-8-10-12 µm amplitude), delivered in a pseudorandom manner.

Go/No-Go vibrotactile task analysis

All analysis was performed with custom-made Python scripts. Behavior was quantified based on the lick events and four main outcomes were measured: Hit and Miss rate for successful and unsuccessful Go trials respectively (number of Hit or Miss divided by the total number of Go trials where a stimulus was delivered), Correct Rejection and False Alarm rate for successful and unsuccessful No-Go trials respectively (number of Correct Rejections or False alarms divided by the total number of No-Go trials). Prestimulus spontaneous licking was calculated as Timeout events during Go trials divided by the total number of Go trials. Training duration was calculated based on the total number of days each animal passed in pre-training and training. For testing, only sessions with less than 40% unsuccessful No-Go trials were analyzed. Psychometric curves were fitted on the Hit rate for each stimulus amplitude using a general linear model. An average of 140 repetitions for each amplitude was used to calculate Hit rates. Detection thresholds were calculated based on the psychometric curves, as the stimulus that the mice detect 50% of the time. Accuracy was calculated based on the slope of the psychometric curve. Sensitivity was calculated as:

$$d' = z(Hit) - z(False\ Alarm)$$

and relative criterion was calculated as:

$$c' = \frac{-1}{2}\frac{\big(z(Hit) + z(FalseAlarm)\big)}{\big(z(Hit) - z(FalseAlarm)\big)}$$

(Detection Theory, Hautus et al).

where z(Hit) is the standard deviation units for Hit rate and z(False Alarm) the standard deviation units for False Alarm rate.

Trial-by-trial variability

Trial-by-trial variability of behavioral responses was measured based on the Hit variance during Go trials for each stimulus amplitude. Normalized trial-by-trial variability was calculated for the threshold (x) amplitude of each mouse, the first amplitude after the threshold (x + 2 µm, suprathreshold) and the first amplitude before the threshold (x - 2 µm, subthreshold).

Clustering of *Fmr1*$^{-/y}$ mice in subgroups

The sci-kit learn implementation of k-means was used on the Hit rates of *Fmr1*$^{-/y}$ mice across all stimulus amplitudes, with 2 clusters targeted and the default parameters.

Adhesive tape removal test

Mice (11-13 weeks old) were handled for one day and underwent three days of gradual habituation to restriction and to a round Plexiglas arena (14 cm diameter) Two patches of adhesive tape were attached to their forepaws as described before (Bouet et al., 2009). The time before the first contact of each tape and the total time necessary for their removal was calculated manually using a Python script.

Two-photon calcium imaging

Setup

Measurements were performed with a Femtonics FEMTOSmart microscope coupled with a widely tunable, femtosecond Ti:Sapphire Laser (Chameleon Ultra, Coherent) pumped by a solid-state laser (Verdi 18W, Coherent). Excitation at 920 nm was used for GCaMP8m and at 1000 nm for mRuby3 and two photomultiplier tubes were used for the collection of green and red fluorescence. Laser power was modulated with pockels cells. A 20x/1 NA objective (Zeiss) was used to obtain 512 × 512 pixel images covering 480 × 480 µm of cortex were acquired at 30.96 Hz using the resonant scanner system (Femtonics). Measurements were written as series of 32 bit images and saved as ome files. Analog and digital inputs sent by Bpod and the piezoelectric sensor controller were collected and saved as timestamps by the microscope and were used to synchronize the behavioral events with the calcium traces from imaging.

Analysis

Measurements were exported in ome files of 2000 frames and converted into tiff files using Fiji (ImageJ). Motion correction, region of interest (ROI) detection and fluorescence extraction was performed using Suite2p (https://suite2p.readthedocs.io/en/latest/index.html) with standard parameters, double registration and denoising. Selection of neurons as ROIs was confirmed through manual curation of the identified ROIs based on shape and calcium traces. To define the inhibitory neurons, colocalization of images obtained for green and red fluorescence was performed using ImageJ. All further analyses were performed separately for excitatory and inhibitory neurons. Custom-made scripts were written in Python to synchronize the behavioral and imaging data and to calculate ΔF/F and z-score values. Neuropil contamination was corrected in all traces before ΔF/F and z-score calculations as:

$$F_{neuropil\text{-}corrected} = F - F_{neuropil} * 0.7.$$

where F is the fluorescence of the neuron (ROI) and $F_{neuropil}$ is the fluorescence of the neuropil associated to the neurons, as calculated by suite2p.

To calculate ΔF/F, baseline fluorescence (F) was calculated for each neuron as the average fluorescence during the 10 s period with the lowest variation (STD) in F.
z-scores were calculated as:

$$z(t) = \frac{\Delta F/F\,(t) - \mu_{prestimbaseline}}{\sigma_{prestimbaseline}}$$

where $\mu_{prestim\ baseline}$ is the mean ΔF/F during the 1 s before stimulation across all trials and $\sigma_{prestim\ baseline}$ is the standard deviation ΔF/F during 1 second before stimulus

All analysis of stimulus-specific responses was conducted in the time window that the stimulus was present, but before the animal's first lick to avoid confounding stimulus- with movement-related activity.

Stimulus-related responses

Stimulus-related activation of a given neuron was computed for each trial by comparing the 85th percentile of the z-score during stimulation to 1,999 random points in the recording (z-score), excluding periods were the stimulus or a reward was delivered. When the z-score during stimulus delivery was higher than the 95th percentile of the 1,999 random points, the neuron was consider activated by the stimulus. A similar method was used for stimulus-related inhibition, comparing the 10th percentile of the z-score during stimulation with 1,999 random points in the recording (z-score). The neuron was considered inhibited by the stimulus if the z-score was lower than -1 * 95th percentile of the 1.999 points. This procedure was adapted from ref[83] constitutes a randomization test at significance level $P < 0.05$.

Response characterization (peak amplitude, peak delay)

Response amplitude was calculated for all neurons that were activated or inhibited during stimulus delivery as the maximum or minimum z-score value during the 500 ms of stimulation. The peak delay was defined as the number of frames between the beginning of stimulus delivery and the peak response amplitude.

Prestimulus activity analysis

Prestimulus activity was calculated as the mean or STD of the z-score, during the 500 ms window before stimulus onset.

Trial-by-trial variability

To estimate the trial-by-trial variability, cosine similarity was calculated between each pair of trials. Trials were represented as vectors. Each neuron was assigned a value of the average z-score fluorescence during stimulus delivery (500 ms) or of its response with the following labels: activated (1), inhibited (-1) or non-responsive (0). Cosine similarity of prestimulus responses was calculated with each neuron assigned a value of its average z-score fluorescence during 500 ms before stimulus onset. For group comparisons the pair-wise matrices were averaged to one single value of cosine similarity for each animal.

Driver neurons

Driver neurons were defined as the neurons that were recruited (activated or inhibited) more than 5 times during detected trials.

Excitation-inhibition (E/I) ratio

E/I ratio was calculated for each trial as the number of activated pyramidal neurons divided by the number of activated GABAergic interneurons.

Decoding of behavioral responses

Dynamic decoding classifiers were adapted from ref.[47], using a logistic regression (Scikit-learn implementation) model with an L2 penalty term to the weights with a regularization strength of 1. Classification accuracy was computed for each frame, with shaded areas are showing the SEM. Decoding accuracy for different time windows was calculated by averaging the accuracy of the frames that constitute each time window across trials. The random undersampling method was used to balance the number of detected/undetected trials, because of the altered Hit/Miss ratio in WT and *Fmr1*$^{-/y}$ mice (Scikit-learn library). This method keeps random trials of the majority class to obtain the same number of trials as in the minority class. Each model was trained in each mouse, to classify the probability of a trial having a Hit or Miss outcome. Four-fold cross validation was used on each session, with a new model trained for each fold for each time-point, and classification accuracy is reported as the average of the test data across folds. A new model was trained from scratch for each imaging frame within a trial; hence, the training data consisted of a vector containing a single scalar ΔF/F value for each cell of all trials on a given frame.

Pharmacology

For rescue experiments, vehicle (standard saline solution, 0.9 M NaCl, supplemented with 1.25% DMSO and 1.25% Tween 80) or BMS-204352 (2 mg per kg, Tocris) were delivered by intraperitoneal injection 30 min before behavioral testing (as described previously Zhang). All mice were first habituated to restriction. Each mouse was treated for 2 days with vehicle and for 2 days with BMS-204352. Testing in the Go/No-Go vibrotactile decision-making task occurred 30 minutes after each treatment, both days. All sessions were included in the analysis (no criterion for sessions with less than 40% unsuccessful No-Go trials was employed).

Histology

Following the end of the experiments, mice were anesthetized with isoflurane (4.5%) and euthanized by cervical dislocation. The brain was extracted, fixed in PFA 4% overnight and washed in 0.1 M PB. Coronal brain slices of 100 mm thickness were obtained using a vibrotome (Leica VT1000 S). Slices were stained with DAPI and the localization of the virus injection in the forepaw-related primary somatosensory cortex was confirmed in a fluorescent microscope (Eclipse Ti-U Nikon).

Statistics

All values are presented as mean ± s.e.m. Box plots show the median, interquartiles, range, mean and individual values. The numbers of animals used are indicated in the figure legends. All statistical analysis was done using Python (SciPy, Pingouin). All datasets were tested for normality. Two-tailed unpaired or paired *t* tests were performed to evaluate the difference between two groups of data. When normal distribution was not confirmed, Mann-Whitney U test was used for comparisons between different groups and Wilcoxon Signed Rank test was used for within-group comparisons. Genotype effects were tested with one-way ANOVA or Kruskal-Wallis ANOVA when more than two groups were present. Genotype and Amplitude or Variance effects were tested with Mixed ANOVA or Friedman test were used for repeated measures analysis.

Blinding and randomization

All experiments and analysis were performed in a blinded manner. Although no randomization was formally applied, the subjects were indeed selected at random due to the blinded nature of the experiments. For pharmacological rescue experiments, equal numbers of *Fmr1*$^{-/y}$ and wild-type mice received BMS-204352 or vehicle. Treatments were evenly assigned within a littermate group.

Code availability

Custom-made Python codes used in this study can be found on the following GitHub repository: https://github.com/OuraniaSem/Percephone.git

Data availability

The raw data of behavioral experiments and calcium imaging generated in this study have been deposited on the figshare database: https://doi.org/10.6084/m9.figshare.26335684.v2
Source data are provided with this paper.

Figures and Figure Legends

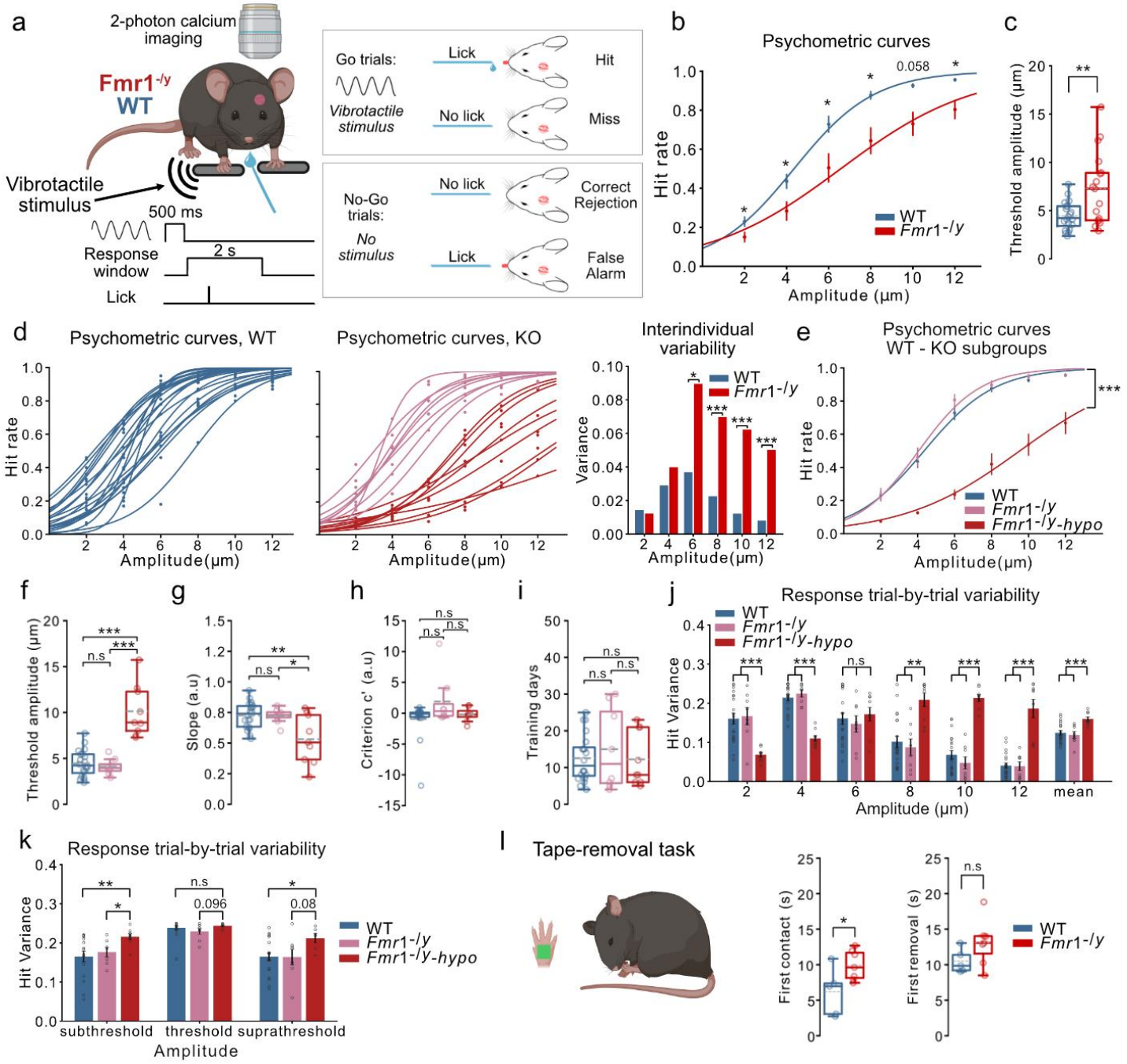

Figure1. **A forepaw-based perceptual decision-making task to assess tactile detection in mice.**

For panels **b, c, d, e, f, g, i, j,:** n=20 WT, 17 *Fmr1*$^{-/y}$ mice (of which 9 *Fmr1*$^{-/y}$-hyposensitive), 5-7 sessions with ~130 repetitions of each amplitude per mouse. For panel **h,:** n=19 WT, 8 *Fmr1*$^{-/y}$, 8 *Fmr1*$^{-/y}$-hyposensitive mice. For panel **k,:** subthreshold: n=16 WT, 7 *Fmr1*$^{-/y}$, 9 *Fmr1*$^{-/y}$-hyposensitive mice, threshold: n=20 WT, 8 *Fmr1*$^{-/y}$, 8 *Fmr1*$^{-/y}$-hyposensitive mice, suprathreshold: n=20 WT, 8 *Fmr1*$^{-/y}$,6 *Fmr1*$^{-/y}$-hyposensitive mice. For panel **l,:** n=5 WT, 7 *Fmr1*$^{-/y}$ mice. **a,** Left: schema showing the behavioral setup and trial protocol. Right: behavioral outcomes depending on the animal's response. **b,** Psychometric curves fitted on average Hit rates for each stimulus amplitude and **(c,)** Detection thresholds calculated based on the psychometric curves. **d,** Psychometric curves of each individual mouse (left and middle, colors depict different groups) and variance of Hit rates (right). **e,** Psychometric curves fitted on average Hit rates for each stimulus amplitude for WT mice and the two Fmr1$^{-/y}$ subgroups. Detection thresholds **(f,)** and perceptual accuracy **(g,)** calculated based on the psychometric curves in **(e,). h**, Relative criterion c' depicting the licking strategy. **i,** Number of days mice spent in pre-training and training. **j,** Trial-by-trial variability calculated as response variance of Hit for each stimulus amplitude and the average for all amplitudes. **k,** Trial-by-trial variability (variance) of Hit responses following normalization for the threshold amplitude of each mouse. Subthreshold stimulus is the first stimulus with amplitude lower than the threshold and suprathreshold stimulus is the first amplitude higher than the threshold. **l,** Left: schema showing the tape removal task. Right: Time (s) until the first contact with the tape and time (s) until the tape removal. P values were computed using Mixed ANOVA for panels **b, e,;** one-way ANOVA for panels **f,-g,;** Kruskal-Wallis ANOVA for panels **h,i,;** Friedman test for panels **j,k,;** two-sided t-test for panels **c, e, f, g, i, j, k, l,**; Mann-Whitney test for panels **b, e, h, i, j, k,**; F test for panel **d**,. ***P < 0.001, **P < 0.01, *P < 0.05 or n.s, not significant.

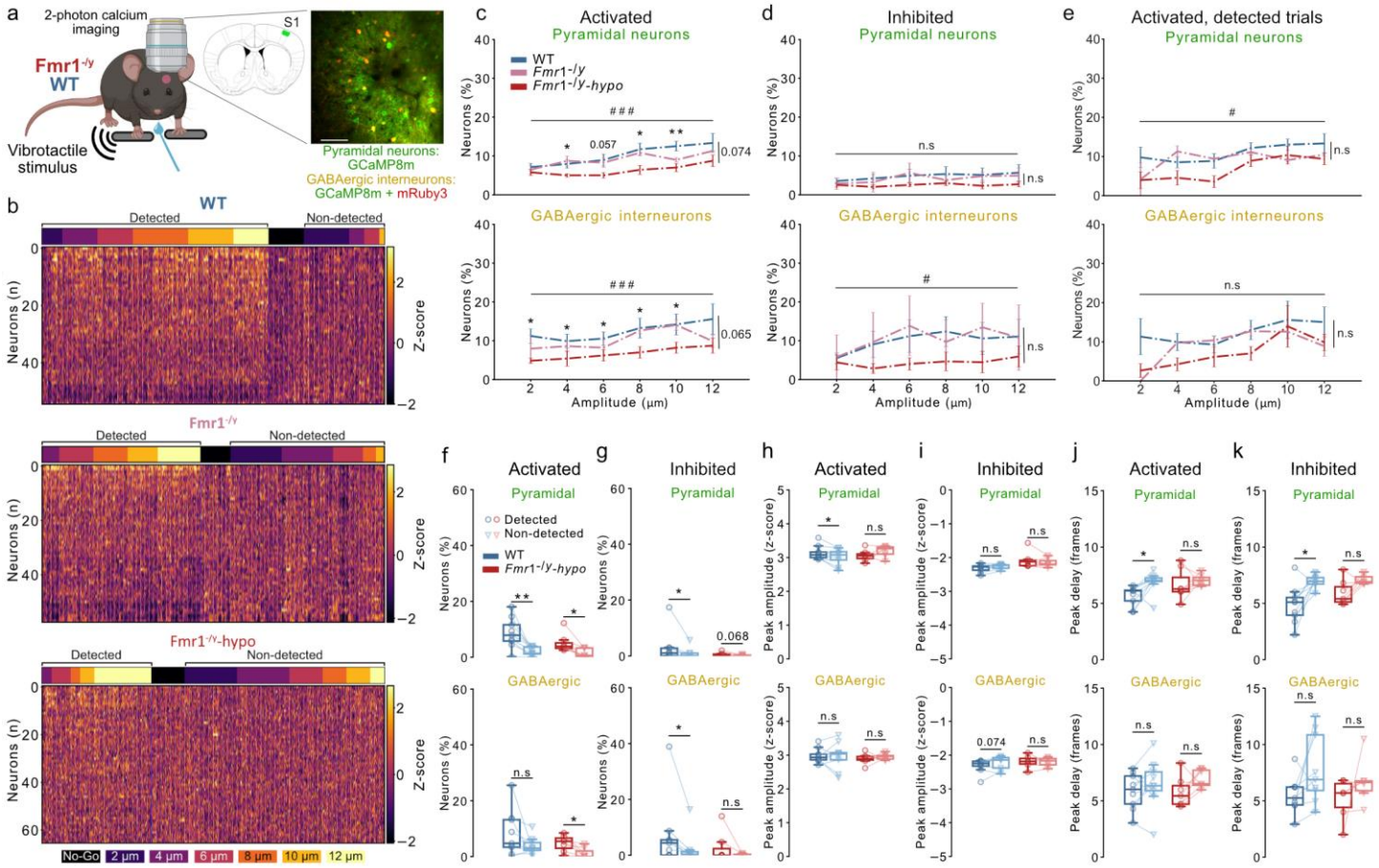

Figure 2. **Weak stimulus encoding in *Fmr1*$^{-/y}$-hyposensitive mice**

For all panels: 1 session, ~10 repetitions of each amplitude per mouse. For panels **c, d, e,:** n=9 WT, 2 *Fmr1*$^{-/y}$ mice, 7 *Fmr1*$^{-/y}$-hyposensitive mice. For panels **f,-k,** (Pyramidal neurons): n=9 WT, 7 *Fmr1*$^{-/y}$-hyposensitive mice. For panels **h, j**, (GABAergic interneurons): n=8 WT, 7 *Fmr1*$^{-/y}$-hyposensitive mice. For panels **i, k,** (GABAergic interneurons): n=9 WT, 6 *Fmr1*$^{-/y}$-hyposensitive mice. **a,** Left: schema showing the imaging setup during tactile detection. Right: Position of injections in the forepaw-related primary somatosensory cortex and example of the field of view (scale bar: 100 mm). GCaMP8m is expressed by excitatory pyramidal neurons and inhibitory GABAergic interneurons. Inhibitory neurons also co-express the red fluorescent marker mRuby3. **b,** Example heat maps of activity (z-score) during stimulus delivery. Each horizontal line depicts a neuron. Vertical white lines indicate the beginning of stimulus delivery. Stimuli are sorted depending on their amplitude and whether they were detected (left) or not (right). No-Go trials are shown in the middle (black). Color-coding of each amplitude is shown at the bottom. **c,** Average percentage of activated pyramidal neurons (top) and GABAergic interneurons (bottom) for each stimulus amplitude. **d,** Same as (**c,**) but for inhibited neurons. **e,** Same as (**c,**) but for activated neurons during detected trials. **f,** Percentage of activated pyramidal neurons (top) and GABAergic interneurons (bottom) in detected (dark color, circles) and non-detected (light-color, triangles) trials. **g,** Same as (**f,**) but for inhibited neurons. **h,** Peak response in z-score amplitude for activated pyramidal neurons (top) and GABAergic interneurons (bottom). **i,** Same as (**h**,) but for inhibited neurons. **j,** Response delay (frames) of the peak amplitude relative to stimulus onset for activated pyramidal neurons (top) and GABAergic interneurons (bottom). **k,** Same as (**j,**) but for inhibited neurons. P values were computed using a mixed ANOVA for panels **c, d, e,**; two-sided t-test for panels **c, d, e,**; two-sided paired t-test for panel **f, h, i, j, k,**; Wilcoxon signed-rank test for panels **f, g, h, i, j**. $^{###}$P < 0.001, $^{\#}$P < 0.05, for amplitude effect. **P < 0.01, *P < 0.05 or n.s, not significant.

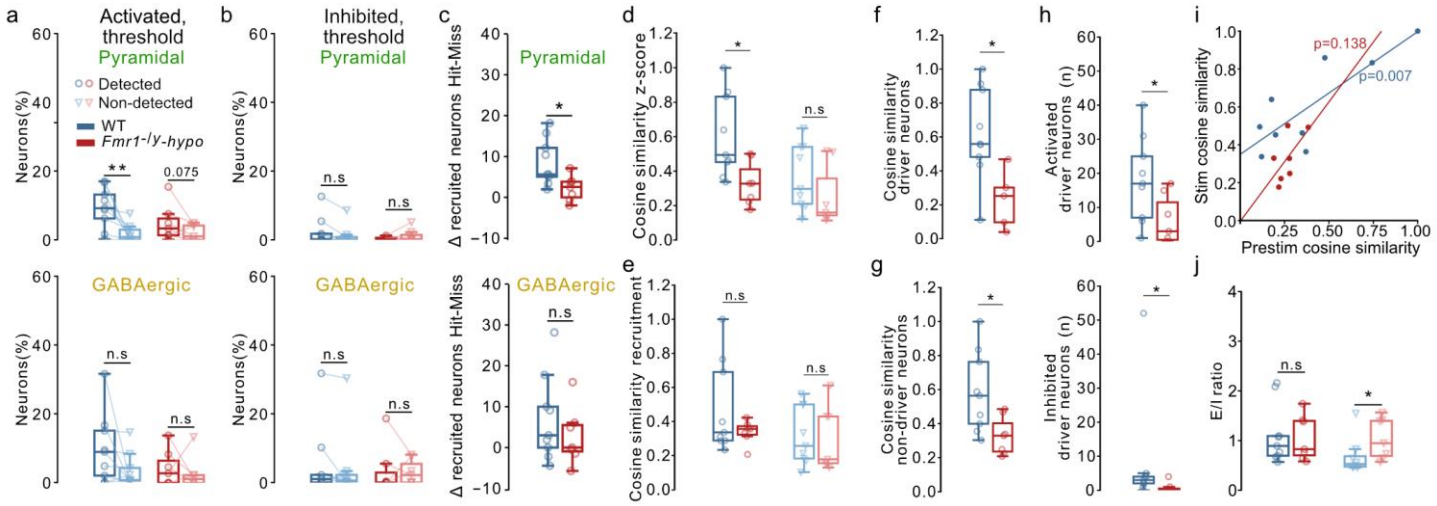

Figure 3. **Response decoding in *Fmr1*$^{-/y}$-hyposensitive mice is vulnerable to the ongoing network state**

For all panels: 1 session, ~10 repetitions of each amplitude per mouse. For all panels apart from **f, j,:** n=9 WT, 7 *Fmr1*$^{-/y}$-hyposensitive mice. For panel **f,:** n=9 WT, 5 *Fmr1*$^{-/y}$-hyposensitive mice. For panel **j,:** Detected: n=9 WT, 8 *Fmr1*$^{-/y}$-hyposensitive mice; Non-detected: n=7 WT, 7 *Fmr1*$^{-/y}$-hyposensitive mice**.** **a,** Percentage of activated pyramidal neurons (top) and GABAegic interneurons (bottom) for the threshold stimulus amplitude of each mouse during detected (dark color, circles) and non-detected trials (light color, triangles). **b,** Same as (**a,**) but for inhibited pyramidal neurons (top) and GABAegic interneurons (bottom). **c,** Δ difference in the percentage of recruited pyramidal neurons (top) and recruited GABAergic interneurons (bottom) between detected (Hit) and non-detected (Miss) trials. **d,** Cosine similarity of the average z-score responses between each pair of detected (dark color, circles) and non-detected (light color, triangles) threshold trials. **e,** Cosine similarity of the identity of recruited neurons between detected (dark color, circles) and non-detected (light color, triangles) threshold trials. **f,** Cosine similarity of the average z-score responses of driver neurons between each pair of detected threshold trials. **g,** same as **(f,)** but for non-driver neurons. **h,** Number of activated (top) and inhibited (bottom) driver neurons in detected threshold trials. **i,** Correlation of cosine similarity of the average z-score responses between each pair of detected threshold trials with the cosine similarity in the prestimulus responses of the same neurons (average z-score, 500 ms). **j,** Excitation/Inhibition (E/I) ratio calculated as number of activated pyramidal neurons divided by the number of activated GABAergic interneurons during detected (dark color, circles) and non-detected trials (light color, triangles). P values were computed using a Wilcoxon signed-rank test for panels **a, b,**; two-sided t-test for panels **c, d, e, f, g, h, j,**; Mann-Whitney test for panels **d, e, h,**; and Pearson correlation coefficient for panel **i.** **P < 0.01, *P < 0.05 or n.s, not significant.

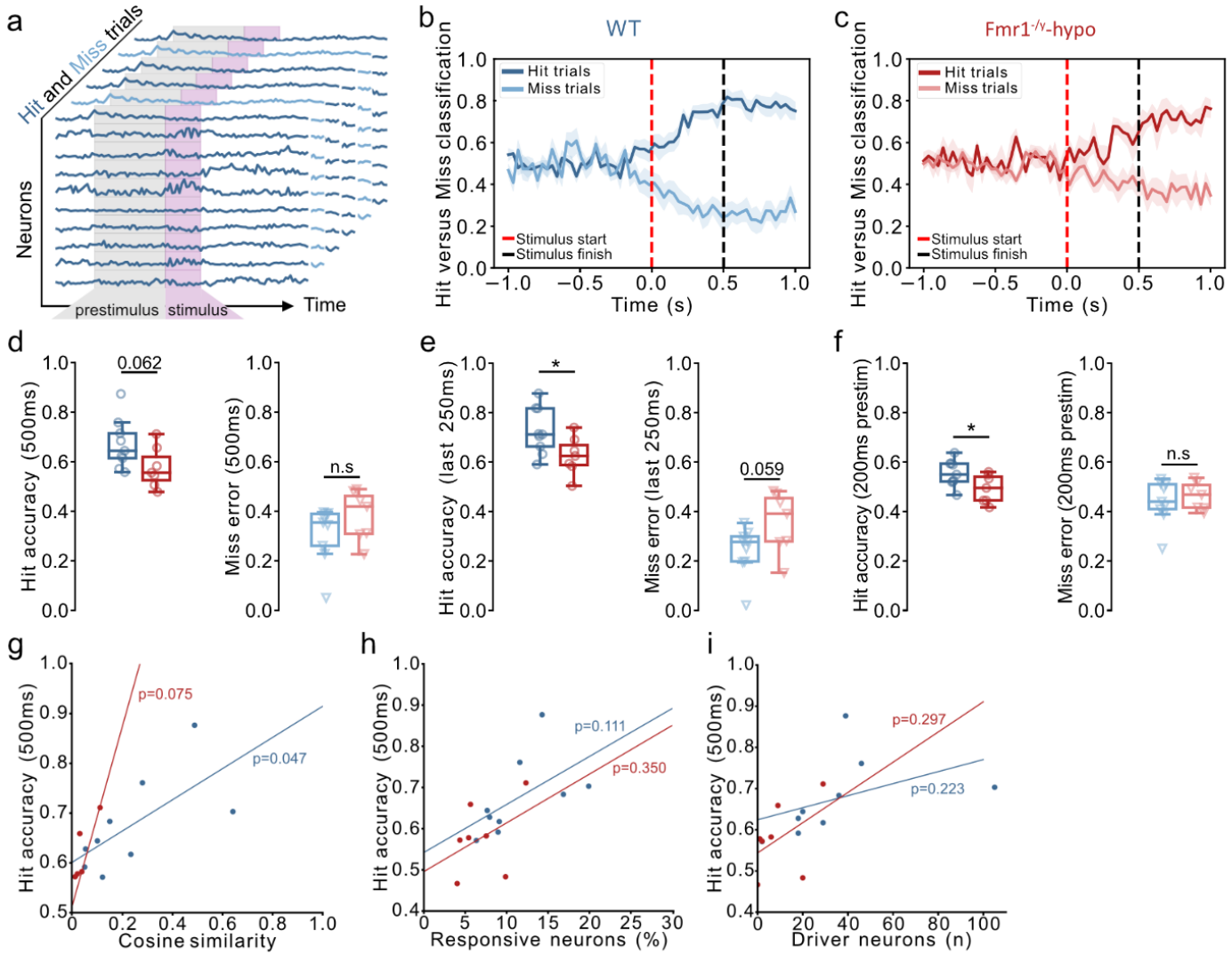

Figure 4. **Unreliable stimulus encoding impedes response decoding in *Fmr1*$^{-/y}$-hyposensitive mice**

For all panels: n=9 WT, 7 *Fmr1*$^{-/y}$-hyposensitive mice, 1 session, ~10 repetitions of each amplitude per mouse. **a,** Schema showing the training strategy of the logistic regression model, with datasets including prestimulus activity (1 s), tactile stimulation (500 ms), post-stimulus activity (500 ms). Classifiers were trained on each frame to decode if the trial was detected (Hit) or non-detected (Miss) (adapted from ref[47]). **b,** Response decoding in WT mice. Stimulus start is indicated by a red dashed line and stimulus end by a black dashed line. The dark-blue line represents true Hit classification and the light-blue line represents false Hit (Miss error) classification. **c,** Same as (**b,**) but for Fmr1$^{-/y}$-hyposensitive mice. **d,** Average Hit accuracy (left) and Miss error (right) of the classifiers on the total duration of the stimulation (500 ms). **e,** Same as (**d,**) but for the last 250 ms of stimulation. **f,** Same as (**d,**) but for the 200 ms prestimulus period before stimulus onset. **g,** Correlation of trial-by-trial similarity (cosine similarity) with the average Hit accuracy of the classifiers during stimulation (500 ms). **h,** Correlation of percentage of responsive neurons with the average Hit accuracy of the classifiers during stimulation (500 ms). **i,** Correlation of the number of driver neurons with the average Hit accuracy of the classifiers during stimulation (500 ms). P values were computed using two-sided t-test for panel **d, e, f,;** Mann-Whitney U test for panel **d, f,;** Pearson correlation coefficient for panels **g, h, i.** *P < 0.05 or n.s, not significant.

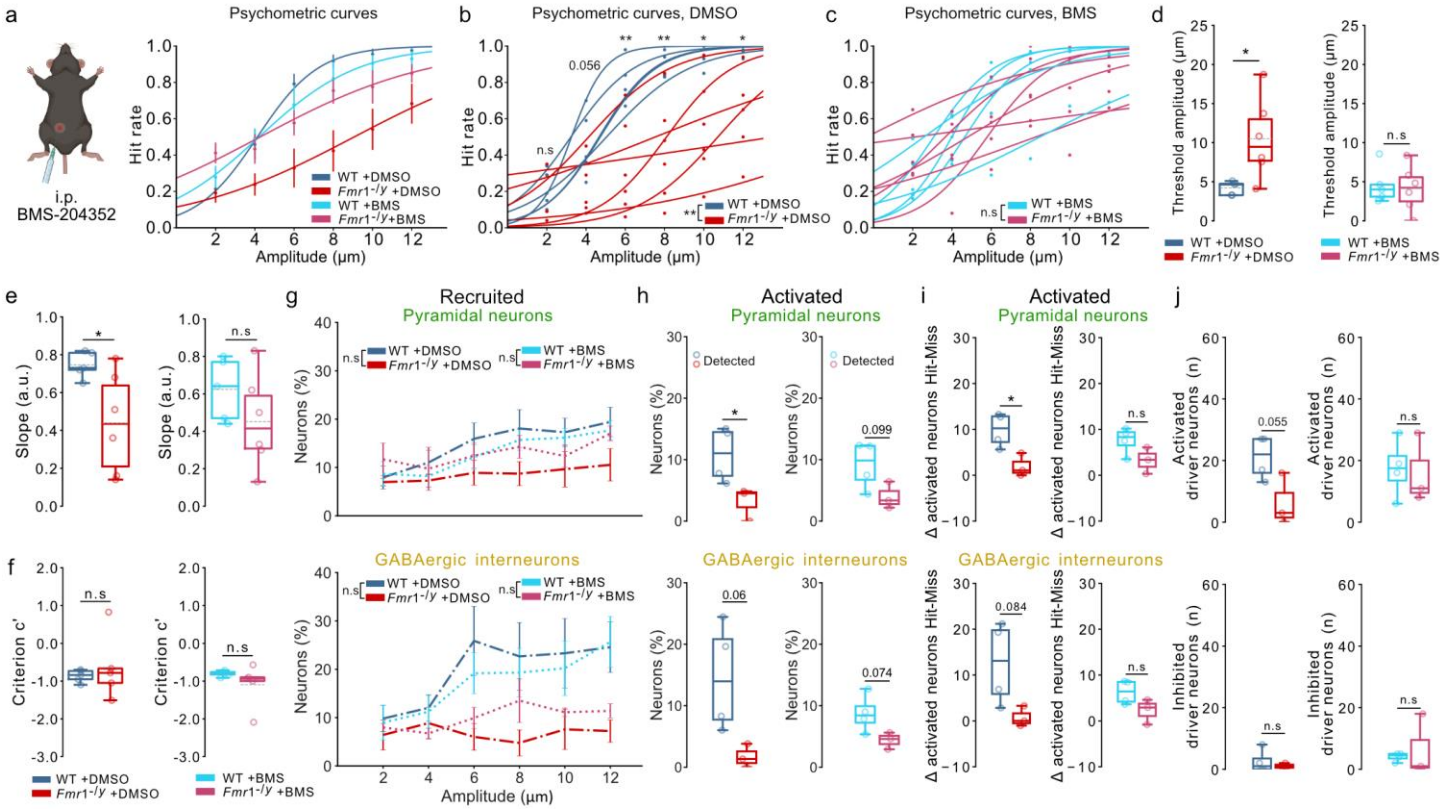

Figure 5. **BK_{CA} agonist improves tactile perception in *Fmr1*$^{-/y}$ mice by enhancing stimulus encoding in S1-FP**

For panels **a,-e,**: n=5 WT, 6 *Fmr1*$^{-/y}$ mice, ~30 repetitions of each amplitude per mouse for DMSO, ~39 repetitions for BMS. For panel **f,**: n=5 WT, 5 *Fmr1*$^{-/y}$ mice, on average ~32 repetitions of each amplitude per mouse for DMSO, ~41 repetitions for BMS. For panels **g,-j,**: n=4 WT, 3 *Fmr1*$^{-/y}$ mice,1 session with ~10 repetitions of each amplitude per mouse for DMSO and BMS. **a,** Left: Intraperitoneal injection of BMS-204352 (BMS). Right: Psychometric curves fitted on average Hit rates for each stimulus amplitude for WT +DMSO (blue), *Fmr1*$^{-/y}$ mice +DMSO (dark red), WT +BMS (cyan) and *Fmr1*$^{-/y}$ mice +BMS (pink). **b,** Psychometric curves of each individual mouse for WT +DMSO (blue), *Fmr1*$^{-/y}$ +DMSO mice (dark red). **c,** Psychometric curves of each individual mouse for WT +BMS (cyan), *Fmr1*$^{-/y}$ +BMS mice (pink). **d,** Detection thresholds calculated based on the psychometric curves with DMSO (left) and BMS treatment (right). **e,** Perceptual accuracy calculated based on the slope of the psychometric curves with DMSO (left) and BMS treatment (right). **f,** Relative criterion c' depicting licking strategy with DMSO (left) and BMS treatment (right). **g,** Average percentage of recruited pyramidal neurons (top) and GABAegic interneurons (bottom) for each stimulus amplitude. **h,** Percentage of activated pyramidal neurons (top) and GABAergic interneurons (bottom) in detected trials. **i,** Δ difference in the percentage of activated pyramidal neurons (top) and GABAergic interneurons (bottom) between detected (Hit) and non-detected (Miss) trials. **j,** Number of activated (top) and inhibited (bottom) driver neurons in detected threshold trials. P values were computed using an one-way ANOVA for panel **b, c,;** a mixed-ANOVA for panel **g**; and a two-sided t-test for panels **b, d, e, f, g, h, i, j**. **P < 0.01, *P < 0.05 or n.s (not significant).

1. American Psychiatric Association. *Diagnostic and statistical manual of mental disorders (5th ed.)*. (2013). doi:https://doi.org/10.1176/appi.books.9780890425596.

2. Balasco, L., Provenzano, G. & Bozzi, Y. Sensory Abnormalities in Autism Spectrum Disorders: A Focus on the Tactile Domain, From Genetic Mouse Models to the Clinic. *Front. Psychiatry* **10**, 1–17 (2020).

3. Foss-Feig, J. H., Heacock, J. L. & Cascio, C. J. Tactile responsiveness patterns and their association with core features in autism spectrum disorders. *Res. Autism Spectr. Disord.* **6**, 337–344 (2012).

4. Thye, M. D., Bednarz, H. M., Herringshaw, A. J., Sartin, E. B. & Kana, R. K. The impact of atypical sensory processing on social impairments in autism spectrum disorder. *Dev. Cogn. Neurosci.* **29**, 151–167 (2018).

5. Zhai, J. *et al.* Correlation and predictive ability of sensory characteristics and social interaction in children with autism spectrum disorder. *Front. Psychiatry* **14**, 1056051 (2023).

6. He, J. L. *et al.* A working taxonomy for describing the sensory differences of autism. *Mol. Autism* **14**, 15 (2023).

7. Baranek, G. T. *et al.* Hyporesponsiveness to Social and Nonsocial Sensory Stimuli in Children with Autism, Children with Developmental Delays, and Typically Developing Children. *Dev. Psychopathol.* **25**, 307 (2013).

8. Haigh, S. M., Minshew, N., Heeger, D. J., Dinstein, I. & Behrmann, M. Over-Responsiveness and Greater Variability in Roughness Perception in Autism. *Autism Res.* **9**, 393–402 (2016).

9. Cascio, C. J., Lorenzi, J. & Baranek, G. T. Self-Reported Pleasantness Ratings and Examiner-Coded Defensiveness in Response to Touch in Children with ASD: Effects of Stimulus Material and Bodily Location. *J. Autism Dev. Disord.* **46**, 1528–1537 (2016).

10. Kadlaskar, G., Seidl, A., Tager-Flusberg, H., Nelson, C. A. & Keehn, B. Atypical Response to Caregiver Touch in Infants at High Risk for Autism Spectrum Disorder. *J. Autism Dev. Disord.* **49**, 2946–2955 (2019).

11. Salkić, N., Ahmetović, Z., Velić, S., Krnojelac, L. & Nazor, V. Difficulties of the tactile sensory system sensory integration of children with autism. *Tech. Soc. Sci. J.* **27**, 502–510 (2022).

12. Cascio, C. *et al.* Tactile perception in adults with autism: a multidimensional psychophysical study. *J. Autism Dev. Disord.* **38**, 127–137 (2008).

13. Puts, N. A. J., Wodka, E. L., Tommerdahl, M., Mostofsky, S. H. & Edden, R. A. E. Impaired tactile processing in children with autism spectrum disorder. *J. Neurophysiol.* **111**, 1803–1811 (2014).

14. Asaridou, M. *et al.* Could Sensory Differences Be a Sex-Indifferent Biomarker of Autism?

Early Investigation Comparing Tactile Sensitivity Between Autistic Males and Females. *J. Autism Dev. Disord.* 1–17 (2022) doi:10.1007/S10803-022-05787-6/FIGURES/6.

15. Güçlü, B., Tanidir, C., Mukaddes, N. M. & Ünal, F. Tactile sensitivity of normal and autistic children. *Somatosens. Mot. Res.* **24**, 21–33 (2007).

16. Marco, E. J. *et al.* Children With Autism Show Reduced Somatosensory Response: An MEG Study. *Autism Res.* **5**, 340–351 (2012).

17. Cascio, C. J., Gu, C., Schauder, K. B., Key, A. P. & Yoder, P. Somatosensory event-related potentials and association with tactile behavioral responsiveness patterns in children with ASD. *Brain Topogr.* **28**, 895 (2015).

18. Puts, N. A. J. *et al.* Reduced GABA and Altered Somatosensory Function in Children with Autism Spectrum Disorder. *Autism Res.* **10**, 608 (2017).

19. Sapey-Triomphe, L. A., Lamberton, F., Sonié, S., Mattout, J. & Schmitz, C. Tactile hypersensitivity and GABA concentration in the sensorimotor cortex of adults with autism. *Autism Res.* **12**, 562–575 (2019).

20. Coskun, M. A. *et al.* How somatic cortical maps differ in autistic and typical brains. *Neuroreport* **20**, 175–179 (2009).

21. Chen, Q. *et al.* Dysfunction of cortical GABAergic neurons leads to sensory hyper-reactivity in a Shank3 mouse model of ASD. *Nat. Neurosci.* **23**, 520–532 (2020).

22. Purves, D. *et al.* Mechanoreceptors Specialized to Receive Tactile Information. (2001).

23. Maricich, S. M., Morrison, K. M., Mathes, E. L. & Brewer, B. M. Rodents Rely on Merkel Cells for Texture Discrimination Tasks. *J. Neurosci.* **32**, 3296 (2012).

24. Abraira, V. E. & Ginty, D. D. The sensory neurons of touch. *Neuron* **79**, 618–639 (2013).

25. Bolton, T. A. W., Freitas, L. G. A., Jochaut, D., Giraud, A. L. & Van De Ville, D. Neural responses in autism during movie watching: Inter-individual response variability co-varies with symptomatology. *Neuroimage* **216**, 116571 (2020).

26. Scheerer, N. E. *et al.* Exploring sensory phenotypes in autism spectrum disorder. *Mol. Autism* **12**, 1–16 (2021).

27. Guo, X. *et al.* Inter-individual heterogeneity of functional brain networks in children with autism spectrum disorder. *Mol. Autism* **13**, 1–13 (2022).

28. Vinçon-Leite, A. *et al.* Identifying interindividual variability of social perception and associated brain anatomical correlations in children with autism spectrum disorder using eye-tracking and diffusion tensor imaging MRI (DTI-MRI). *Cereb. Cortex* **34**, (2024).

29. Valiquette, V. *et al.* Examining litter specific variability in mice and its impact on neurodevelopmental studies. *Neuroimage* **269**, (2023).

30. Bechard, A., Nicholson, A. & Mason, G. Litter Size Predicts Adult Stereotypic Behavior in

Female Laboratory Mice. *J. Am. Assoc. Lab. Anim. Sci.* **51**, 407 (2012).

31. Healy, K., McNally, L., Ruxton, G. D., Cooper, N. & Jackson, A. L. Metabolic rate and body size are linked with perception of temporal information. *Anim. Behav.* **86**, 685–696 (2013).

32. Dinuzzo, M. *et al.* Perception is associated with the brain's metabolic response to sensory stimulation. *Elife* **11**, (2022).

33. Giulivi, C. *et al.* Mitochondrial dysfunction in autism. *JAMA* **304**, 2389–2396 (2010).

34. Dhillon, S., A. Hellings, J. & G. Butler, M. Genetics and mitochondrial abnormalities in autism spectrum disorders: a review. *Curr. Genomics* **12**, 322–332 (2011).

35. Goh, S., Dong, Z., Zhang, Y., DiMauro, S. & Peterson, B. S. Mitochondrial dysfunction as a neurobiological subtype of autism spectrum disorder: evidence from brain imaging. *JAMA psychiatry* **71**, 665–671 (2014).

36. Barone, R. *et al.* Mitochondrial Fatty Acid β-Oxidation and Resveratrol Effect in Fibroblasts from Patients with Autism Spectrum Disorder. *J. Pers. Med.* **11**, (2021).

37. Frye, R. E. *et al.* Mitochondria May Mediate Prenatal Environmental Influences in Autism Spectrum Disorder. *J. Pers. Med.* **11**, (2021).

38. Noel, J. P., Lakshminarasimhan, K. J., Park, H. & Angelaki, D. E. Increased variability but intact integration during visual navigation in Autism Spectrum Disorder. *Proc. Natl. Acad. Sci. U. S. A.* **117**, 11158–11166 (2020).

39. Wang, Q. *et al.* Investigating intra-individual variability of face scanning in autistic children. *https://doi.org/10.1177/13623613211064373* **26**, 1752–1764 (2021).

40. Milne, E. Increased intra-participant variability in children with autistic spectrum disorders: Evidence from single-trial analysis of evoked EEG. *Front. Psychol.* **2**, 1–12 (2011).

41. Dinstein, I. *et al.* Unreliable Evoked Responses in Autism. *Neuron* **75**, 981–991 (2012).

42. Kovarski, K. *et al.* Reduced visual evoked potential amplitude in autism spectrum disorder, a variability effect? *Transl. Psychiatry* **9**, (2019).

43. Bouet, V. *et al.* The adhesive removal test: a sensitive method to assess sensorimotor deficits in mice. *Nat. Protoc.* **4**, 1560–1565 (2009).

44. Green, D., & Swets, J. *Signal detection theory and psychophysics*. (John Wiley, 1966).

45. Gescheider, G. A. *Psychophysics (3rd ed.). Psychology Press* (1997).

46. Bhaskaran, A. A. *et al.* Endogenous noise of neocortical neurons correlates with atypical sensory response variability in the Fmr1−/y mouse model of autism. *Nat. Commun. 2023 141* **14**, 1–16 (2023).

47. Rowland, J. M. *et al.* Propagation of activity through the cortical hierarchy and perception are determined by neural variability. *Nat. Neurosci.* **26**, 1584–1594 (2023).

48. Rubenstein, J. L. R. & Merzenich, M. M. Model of autism: Increased ratio of excitation/inhibition in key neural systems. *Genes, Brain Behav.* **2**, 255–267 (2003).

49. Pereira, M. *et al.* Evidence accumulation relates to perceptual consciousness and monitoring. *Nat. Commun. 2021 121* **12**, 1–11 (2021).

50. Laumonnier, F. *et al.* Association of a functional deficit of the BKCa channel, a synaptic regulator of neuronal excitability, with autism and mental retardation. *Am. J. Psychiatry* **163**, 1622–1629 (2006).

51. Deng, P. Y. *et al.* FMRP Regulates Neurotransmitter Release and Synaptic Information Transmission by Modulating Action Potential Duration via BK channels. *Neuron* **77**, 696 (2013).

52. Guglielmi, L. *et al.* Update on the implication of potassium channels in autism: K(+) channelautism spectrum disorder. *Front. Cell. Neurosci.* **9**, (2015).

53. Zhang, Y. *et al.* Dendritic channelopathies contribute to neocortical and sensory hyperexcitability in Fmr1-/y mice. *Nat. Neurosci.* **17**, 1701–1709 (2014).

54. Carreno-Munoz, M. I. *et al.* Potential Involvement of Impaired BKCa Channel Function in Sensory Defensiveness and Some Behavioral Disturbances Induced by Unfamiliar Environment in a Mouse Model of Fragile X Syndrome. *Neuropsychopharmacology* **43**, 492–502 (2018).

55. Ferraguto, C., Bouleau, Y., Peineau, T., Dulon, D. & Pietropaolo, S. Hyperacusis in the Adult Fmr1-KO Mouse Model of Fragile X Syndrome: The Therapeutic Relevance of Cochlear Alterations and BKCa Channels. *Int. J. Mol. Sci.* **24**, 11863 (2023).

56. Scott, K. E. *et al.* Closing the species gap: Translational approaches to studying sensory processing differences relevant for autism spectrum disorder. *Autism Res.* **14**, 1322–1331 (2021).

57. Tillmann, J. *et al.* Dissecting the phenotypic heterogeneity in sensory features in autism spectrum disorder: A factor mixture modelling approach. *Mol. Autism* **11**, 1–15 (2020).

58. Scheerer, N. E. *et al.* Exploring sensory phenotypes in autism spectrum disorder. *Mol. Autism* **12**, 1–16 (2021).

59. Orefice, L. L. L. *et al.* Peripheral Mechanosensory Neuron Dysfunction Underlies Tactile and Behavioral Deficits in Mouse Models of ASDs. *Cell* **166**, 299–313 (2016).

60. Orefice, L. L. *et al.* Targeting Peripheral Somatosensory Neurons to Improve Tactile-Related Phenotypes in ASD Models. *Cell* **178**, 867-886.e24 (2019).

61. Deemyad, T. *et al.* Lateralized Decrease of Parvalbumin+ Cells in the Somatosensory Cortex of ASD Models Is Correlated with Unilateral Tactile Hypersensitivity. *Cereb. Cortex*

32, 554–568 (2022).

62. He, C. X. *et al.* Tactile defensiveness and impaired adaptation of neuronal activity in the Fmr1 knock-out mouse model of autism. *J. Neurosci.* **37**, 6475–6487 (2017).

63. Haznedar, M. M. *et al.* Limbic circuitry in patients with autism spectrum disorders studied with positron emission tomography and magnetic resonance imaging. *Am. J. Psychiatry* **157**, 1994–2001 (2000).

64. Lumaban, J. G. & Nelson, D. L. The Fragile X proteins Fmrp and Fxr2p cooperate to regulate glucose metabolism in mice. *Hum. Mol. Genet.* **24**, 2175 (2015).

65. Licznerski, P. *et al.* ATP Synthase c-Subunit Leak Causes Aberrant Cellular Metabolism in Fragile X Syndrome. *Cell* **182**, 1170-1185.e9 (2020).

66. Cohen, L. G., Bandinelli, S., Sato, S., Kufta, C. & Hallett, M. Attenuation in detection of somatosensory stimuli by transcranial magnetic stimulation. *Electroencephalogr. Clin. Neurophysiol.* **81**, 366–376 (1991).

67. McKay, D. R., Ridding, M. C. & Miles, T. S. Magnetic stimulation of motor and somatosensory cortices suppresses perception of ulnar nerve stimuli. *Int. J. Psychophysiol.* **48**, 25–33 (2003).

68. Tamè, L. & Holmes, N. P. Involvement of human primary somatosensory cortex in vibrotactile detection depends on task demand. *Neuroimage* **138**, 184–196 (2016).

69. Pérez-Ortega, J., Akrouh, A. & Yuste, R. Stimulus encoding by specific inactivation of cortical neurons. *Nat. Commun. 2024 151* **15**, 1–14 (2024).

70. Dalgleish, H. W. P. *et al.* How many neurons are sufficient for perception of cortical activity? *Elife* **9**, 1–99 (2020).

71. Park, W. J., Schauder, K. B., Zhang, R., Bennetto, L. & Tadin, D. High internal noise and poor external noise filtering characterize perception in autism spectrum disorder. *Sci. Rep.* **7**, (2017).

72. Yang, H., Kwon, S. E., Severson, K. S. & O'Connor, D. H. Origins of choice-related activity in mouse somatosensory cortex. *Nat. Neurosci.* **19**, 127 (2016).

73. Finkel, E. A. *et al.* Tactile processing in mouse cortex depends on actioncontext. *Cell Rep.* **43**, 113991 (2024).

74. Antoine, M. W., Langberg, T., Schnepel, P. & Feldman, D. E. Increased Excitation-Inhibition Ratio Stabilizes Synapse and Circuit Excitability in Four Autism Mouse Models. *Neuron* **101**, 648-661.e4 (2019).

75. Michaelson, S. D. *et al.* SYNGAP1 heterozygosity disrupts sensory processing by reducing touch-related activity within somatosensory cortex circuits. *Nat. Neurosci.* **21**, (2018).

76. Contractor, A., Klyachko, V. A. & Portera-Cailliau, C. Altered neuronal and circuit excitability in Fragile X Syndrome. *Neuron* **87**, 699 (2015).

77. Carandini, M. & Heeger, D. J. Normalization as a canonical neural computation. *Nat. Rev. Neurosci.* **13**, 51 (2012).

78. Haigh, S. M., Heeger, D. J., Dinstein, I., Minshew, N. & Behrmann, M. Cortical variability in the sensory-evoked response in autism. *J. Autism Dev. Disord.* **45**, 1176 (2015).

79. Hébert, B. *et al.* Rescue of fragile X syndrome phenotypes in Fmr1 KO mice by a BKCa channel opener molecule. *Orphanet J. Rare Dis.* **9**, (2014).

80. Lane, A. E., Molloy, C. A. & Bishop, S. L. Classification of Children With Autism Spectrum Disorder by Sensory Subtype: A Case for Sensory-Based Phenotypes. *Autism Res.* **7**, 322–333 (2014).

81. Lyons-Warren, A. M., Wangler, M. F. & Wan, Y.-W. Cluster Analysis of Short Sensory Profile Data Reveals Sensory-Based Subgroups in Autism Spectrum Disorder. *Int. J. Mol. Sci.* **23**, 13030 (2022).

82. Frye, R. E., Rose, S., Boles, R. G. & Rossignol, D. A. A Personalized Approach to Evaluating and Treating Autism Spectrum Disorder. *J. Pers. Med.* **12**, (2022).

83. Prsa, M., Morandell, K., Cuenu, G. & Huber, D. Feature-selective encoding of substrate vibrations in the forelimb somatosensory cortex. *Nature* **567**, 384–388 (2019).

Acknowledgments

We would like to thank the animal housing and genotyping facilities of INSERM U1215 Neurocenter Magendie. We thank Apolline Joliot for assisting in immunohistochemistry experiments. We thank Dr. James Poulet (Max-Delbrück-Centrum für Molekulare Medizin, Berlin) for providing the capacitive sensors for the behavioral task. This project was funded by the Foundation for Medical Research Postdoc Fellowship (O.S.), INSERM (A.F.), Marcel Dassault-Fondation FondaMental Award 2019 (A.F.), Simons Foundation Autism Research Initiative (A.F.), GIS Autisme & TND (O.S.), Fondation FondaMental.

Author Information

Authors and Affiliations
INSERM, U1215 Neurocentre Magendie, 33077, Bordeaux, France
Semelidou Ourania, Théo Gauvrit, Célien Vandromme, Alexandre Cornier, Anna Saint-Jean, Yves Le Feuvre, Melanie Ginger, Andreas Frick
University of Bordeaux, 33000, Bordeaux, France
Semelidou Ourania, Théo Gauvrit, Célien Vandromme, Alexandre Cornier, Anna Saint-Jean, Yves Le Feuvre, Melanie Ginger, Andreas Frick
University of Lille, 59000 , Lille, France
Célien Vandromme

Contributions

A.F., M.G., and O.S. conceived the project and designed the experiments. O.S. performed the experiments. A.S.J. and Y.L.F. contributed to the tape removal experiments and their analysis. A.C. wrote the Python code for the behavioral experiments. O.S., T.G., and C.V. analyzed the data and wrote the necessary Python scripts. O.S. prepared the figures. O.S., T.G., and A.F. interpreted the data. O.S. wrote the manuscript, and A.F., M.G., Y.L.F., and T.G. provided feedback.

Corresponding author

Correspondence to Andreas Frick and Ourania Semelidou.

Ethics declarations

Competing interests

The authors declare no competing interests.

Inclusion and diversity statement

We support inclusive, diverse, and equitable conduct of research. We tried to use inclusive language as much as possible.